



# Effect of severe shot peening on the fatigue life of the laser-cladded Inconel 718 specimens

Mir Siavash Ghorashi<sup>1</sup> · Gholam Hossein Farrahi<sup>1</sup> · Mohammad Reza Movahhedy<sup>1</sup>

Received: 14 February 2019 / Accepted: 26 June 2019 / Published online: 17 July 2019  
© Springer-Verlag London Ltd., part of Springer Nature 2019

## Abstract

This paper presents the influence of the severe shot peening process on the fatigue life of the laser-cladded Inconel 718 specimens which can be employed during refurbishment of components enduring high mechanical cyclic loads such as gas turbine components. In order to quantitatively evaluate the destructive effect of laser cladding on the fatigue endurance, fatigue tests are first performed on the as-received and laser-cladded specimens. Then, microstructural analysis by scanning electron microscope (SEM) is carried out to identify the root causes of the drawback of laser cladding. Moreover, by employing a comprehensive laser-cladding FE analysis considering cyclic plastic material modeling, the induced residual stress distribution is determined. To decrease the detrimental effects of laser cladding on the microstructure and residual stresses, the specimens are next subjected to severe shot peening treatment, and then, extra sets of fatigue tests are conducted on the specimens. The conducted experiments show that the laser cladding can cause the deterioration of the fatigue life of the specimens at about 40%, and the damaged fatigue life can be almost restored by the severe shot peening. The experiments also indicate that the clad-toe zone is the weakest area concerning fatigue issues in laser-cladded specimens with or without shot peening post-process. Hence, the clad-toe zone needs some special attention.

**Keywords** Laser cladding · Severe shot peening · Fatigue life · Cyclic plasticity · Inconel 718 · Residual stress

## 1 Introduction

Laser-cladding process is one of the advanced prevalent technologies for surface modification and repair of critical load-bearing components in which a thin layer of filler material with the desired properties is deposited on the surface of a substrate by utilizing a laser as the heat source. Laser cladding has acquired widespread acceptance among industrial researchers in recent years due to its prominent features such as low dilution, good metallurgical bonding at the interface, high deposition accuracy, fine resulted microstructure, fast heating and cooling rates, shallow heat-affected zone, and low distortion. It is to be noted that despite the advantages of laser-cladding technique, during this surface engineering process, tensile residual stresses are generated which may lead

to destructive consequences like crack propagation, undesirable deformation, and reduced fatigue strength.

In order to have a review, the conducted investigations on the laser cladding and its effect regarding fatigue life and the modifying post-processes to treat the detrimental effect of laser cladding, three different research categories are presented in the following order. First, the investigations focused on the effect of laser cladding on the fatigue life of specimens are discussed. Then, some post-processing techniques, which have the potential to enhance the fatigue life of laser-cladded (LC) specimens by cancelling out the detrimental effect of tensile residual stress field of laser cladding, are described. Finally, a few investigations utilizing FE analysis to simulate this process in order to achieve the resulted residual stresses are also stated.

Several researchers have studied the fatigue performance of LC components. Ganesh et al. [1] investigated the fatigue crack propagation and fracture toughness of the laser-fabricated Inconel 625 compact tension specimens. X-ray diffraction patterns obtained on the fatigue fracture surfaces of specimens revealed strong (1 1 1) texture indicating preferential presence of (1 1 1) planes on the fracture surface. It was

✉ Gholam Hossein Farrahi  
farrahi@sharif.edu

<sup>1</sup> School of Mechanical Engineering, Sharif University of Technology, Tehran, Iran

also confirmed from the XRD patterns that the slip plane (1 1 1) mainly existed parallel to the growth direction due to solidification texture. From these observations, they concluded that the crack grew in the growth direction mainly along the (1 1 1) planes [1]. Chew and Pang [2] presented a fatigue crack growth model for multiple fatigue cracks propagating from the clad-toe region of LC AISI 4340 steel specimens. Their fatigue life prediction results were in a good agreement with the experimental S-N curve test data. By means of self-restrain thermal fatigue test, Tong et al. [3] studied the thermal fatigue strength of non-smooth cast iron LC specimens by different self-fluxing alloys. In addition, they surveyed the microstructures and phase structures of non-smooth units by employing scanning electron microscope (SEM) and XRD. By conducting rotary bending fatigue tests on some LC specimens made of AISI 4130 steel, Hutasoit et al. [4] indicated that the fatigue life of the specimens is lower comparing with the specimens without cladding. Lourenco et al. [5] reported several microstructure analyses and residual stress data in a study of the influence of the laser-cladding process on the fatigue performance of a certain type of ultra-high strength steel. Chew et al. [6] experimentally verified that pre-clad groove machining and post-clad surface grinding processes increase the fatigue strength of specimens made of AISI 4340 steel comparing with as-clad specimens. By conducting the roller-on-disc tests, Roy et al. [7] studied the influence of deposition material type and heat treatment process on the rolling contact fatigue performance of LC steel rails.

To improve the fatigue strength of components and parts, some surface modification techniques such as shot peening, laser shock peening (LSP), ultrasonic impact peening, and deep surface rolling would be beneficial. Klotz et al. [8] conducted uniaxial force-controlled fatigue tests to determine the

influence of different shot peening conditions on the low- and high-cycle fatigue responses of the Inconel 718 specimens. A comparison between the effects of metallic shot peening and LSP on the microstructure and induced residual stress field of the Ti-6Al-4V specimens has been made by Lainé et al. [9]. They utilized incremental center hole drilling for measuring residual stress distribution and used SEM and TEM for microstructural analysis to show that LSP influences lower depths and gives more severe deformation comparing with the metallic shot peening. The good LSP effects on the laser additive manufacture TC17 Ti alloy in regaining fatigue strength have been studied by Luo et al. [10] with utilization of XRD to measure residual stress field and SEM to analyze the microstructure of LC specimens. Using the post-processing method of deep surface rolling, Zhuang et al. [11] studied the associated effects on the fatigue life of LC 7075-T651 aluminum alloy specimens. Their results showed that this post-processing method enhances fatigue life considerably in comparison with the as-clad specimens. Ramos et al. [12] conducted the surface modification method of ultrasonic impact peening on some specimens of Al7075-T7351 and the metallic shot peening process on some other specimens of the same material to study the effects of each one of these two processes regarding the fatigue life. They showed while the shot peening enhances the fatigue life slightly more than the ultrasonic impact peening, the latter left much lower surface roughness.

In the present research, the shot peening method is chosen as a post-process on LC specimens to study its effect on the deteriorated fatigue life, with noting that to the authors' best knowledge, the effectiveness of this post-process for LC components has not been investigated yet. The cold working surface treatment of shot peening is already broadly used to

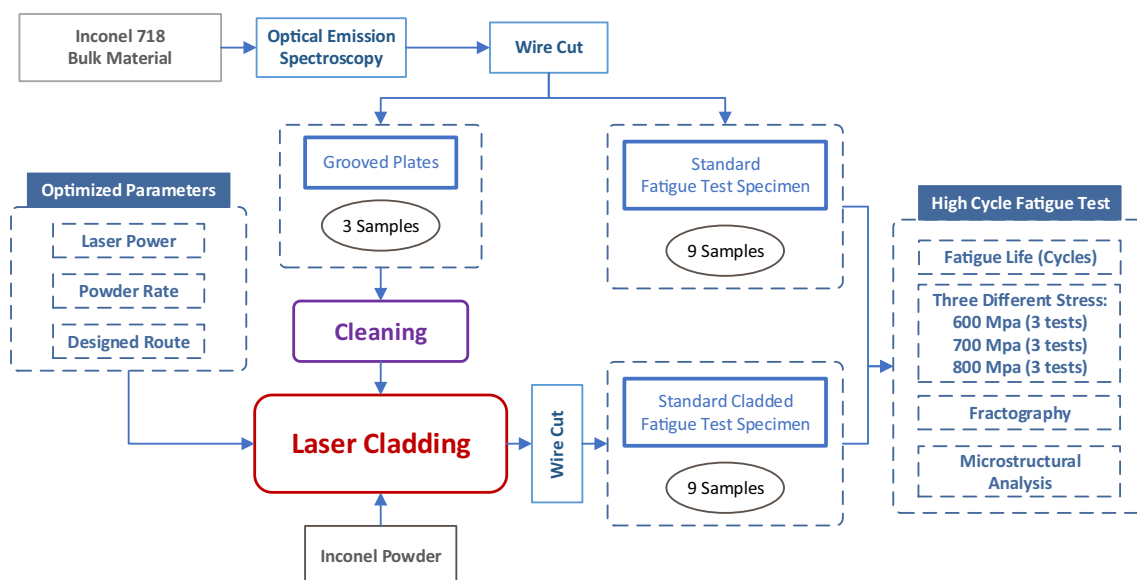


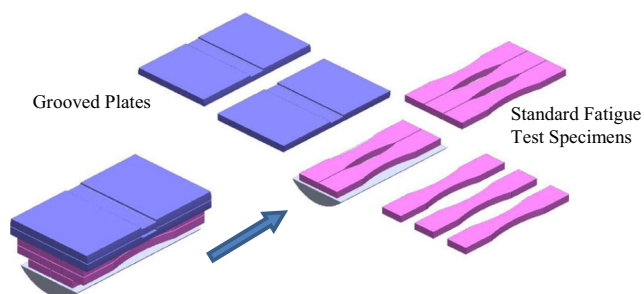
Fig. 1 Flowchart of the laser-cladding experiment design

**Table 1** Chemical composition of the prepared Inconel 718 material (wt%)

C	Mn	Cr	Mo	Fe	Zr	Si	P	S
0.038	< 0.0003	17.77	2.84	19.99	0.0105	0.0344	0.005	< 0.0011
V	Al	Nb	Cu	Ta	Ti	Co	B	Ni
0.0117	0.534	4.85	0.0318	0.0429	0.927	0.0907	0.0048	Bal.

enhance the fatigue life of mechanical components in many cases. As an example, Zhang and Lindemann [13] studied the effect of shot peening on the fatigue behavior of wrought magnesium alloy AZ80. They showed that with a certain shot peening parameters, an improvement of 60% in the fatigue strength can be achieved. Bagherifard and Guagliano [14] experimentally investigated the fatigue performance of low-alloy steel specimens treated by severe shot peening. Seddik et al. [15] proposed a model to predict the high-cycle fatigue limit of shot-peened parts. They used a three-step model to predict the fatigue life of a shot-peened Waspaloy part. By performing the 4-point bending fatigue test, Sidhom et al. [16] studied the high-cycle fatigue resistance of shot-peened 5083 H11 Al-alloy T-welded joints. They experimentally determined the induced effects of the welding in the critical region of weld-toe both before and after the shot peening. Habibi et al. [17] studied the shot peening-related fatigue strength improvement of welded tubular X-joint of an offshore structure. In the work of Lago et al. [18], the fatigue life enhancement of welded S355 J2 steel by severe shot peening has been experimentally demonstrated. Benchouia et al. [19] also evaluated the effect of stress ratio and shot peening on the fatigue life of welded AISI 304L stainless steel. They have found that the shot peening post-welding process improves the fatigue life and microhardness of treated materials.

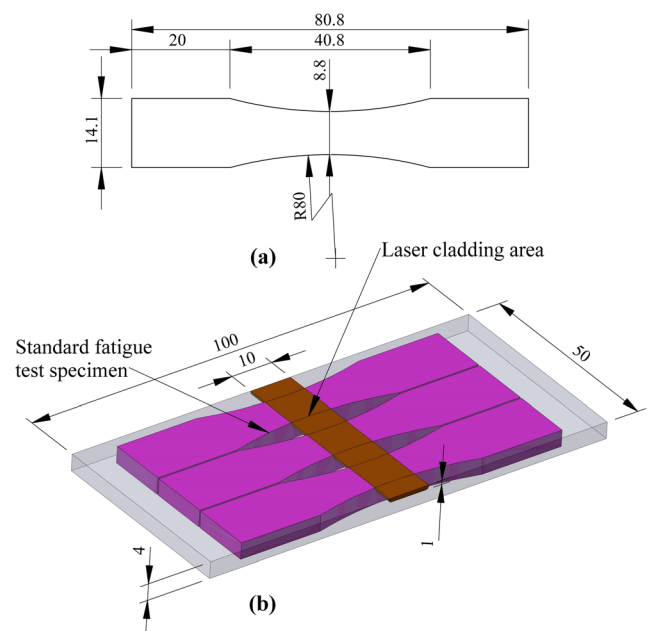
Finite element analysis is widely used to simulate the laser-cladding process in order to predict the residual stresses distribution, which plays an important role regarding the fatigue endurance of the specimens. As an instance, Nazemi et al. [20] predicted the temperature history and residual stress field caused by laser cladding of P420 stainless steel powder on AISI 1018 plates. In a FE simulation of laser deposition of Inconel 718 powder on Ti-6Al-4V substrate, Shah et al. [21] also estimated the residual stress distribution at the clad region

**Fig. 2** Schematic of the grooved plates and standard specimens

together with the interface of cladding and the substrate, and compared their estimation with XRD data.

In this study, the effectiveness of the severe shot peening treatment for enhancement of fatigue endurance of the Inconel 718 LC specimens is evaluated, mainly based on experimental investigation. The term “severe shot peening” or “high-energy shot peening” stands for the process in which significant grain refinement on the surface of the specimens is resulted [22]. By increasing the kinetic energy of the shot impacts, by applying high intensity and high coverage, severe plastic deformation can be achieved. The result will be the refinement of the grains.

To this purpose, first, a set of uniaxial fatigue tests is conducted to compare the fatigue life of the as-received and LC specimens. These comparisons indicate the drawback of laser cladding regarding the fatigue issues. To have an insight for this drawback, microstructural investigation and FE analysis are carried out. For the microstructural investigation, some metallographic samples are prepared and etched from different regions of the LC specimens, including substrate, clad-and-substrate interface, and clad-toe zone, to be investigated by SEM. A FE model is also developed by considering various aspects of the laser-cladding process, including the cyclic

**Fig. 3** a Standard fatigue test specimen dimensions. b LC grooved plate cut into 3 standard fatigue test specimens

plasticity behavior of the material due to cyclic thermal stresses and non-linear kinematic hardening behavior of the material based on the Armstrong-Frederick plasticity model [23], to accurately analyze the residual stress distribution in the specimens. In the final step of the study, a set of LC specimens are shot peened. In order to investigate the effect of the shot peening process, as a promising treatment on the fatigue life enhancement, a set of fatigue tests is carried out on the shot-peened specimens.

## 2 Materials and methods

### 2.1 Design of laser-cladding experiment

An overall view of the experiment design to conduct the high-cycle fatigue (HCF) tests on the as-received and laser-cladded (LC) Inconel 718 specimens is shown in Fig. 1. This experiment is designed in order to provide some data in comparing the fatigue strength of these two sets of specimens with each other. In the following section, the steps of this experimental activity are described.

### 2.2 HCF specimen preparation

The provided bulk material, in the shape of a rod with 50 mm diameter, is first analyzed to ensure that the chemical

composition is in agreement with Inconel 718. The chemical composition for the provided material is shown in Table 1.

Then, “the grooved plates” and “the standard fatigue test specimens,” schematically shown in Fig. 2, are built by wire cutting. All the surfaces of the parts are then polished to remove surface irregularities caused by wire cutting.

The fatigue tests on the specimens with continuous radius between ends, which their dimensions are shown in Fig. 3a, are conducted according to the ASTM E466 standard practice [24]. The groove in the middle of a grooved plate has the role of an artificial damage to the base material which in next steps will be filled thoroughly by the laser-cladding process to restore the geometry. After cladding, by wire cutting, each of these plates is split into three standard fatigue test specimens (please see Fig. 3b).

### 2.3 Laser-cladding process parameters

Instruments used for laser cladding in this investigation were a 700-W Nd:YAG laser equipped with a coaxial nozzle, a two-axis CNC work station, and an automatic powder feeder. Specimens were completely cleaned by acetone before cladding. The used process parameters of cladding are presented in Table 2. The laser beam in the cladding process moved in the pattern shown in Fig. 4 to produce clad beads with 66% transverse overlapping to have a relatively flat clad. The clad bead section is shown in Fig. 4.

**Fig. 4** The pattern of cladding and the clad bead section

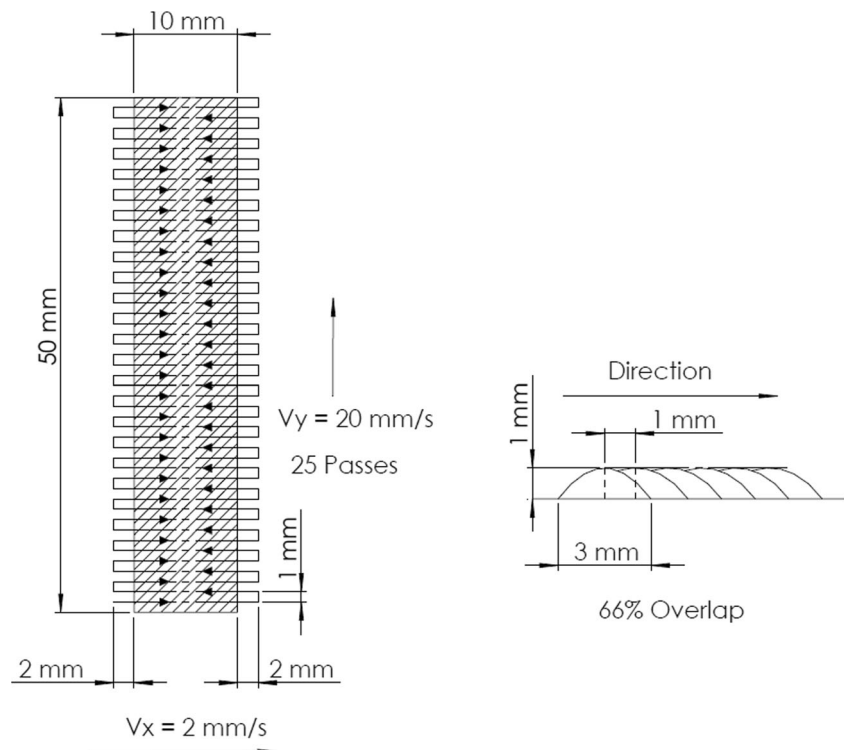


**Table 2** Laser-cladding parameters

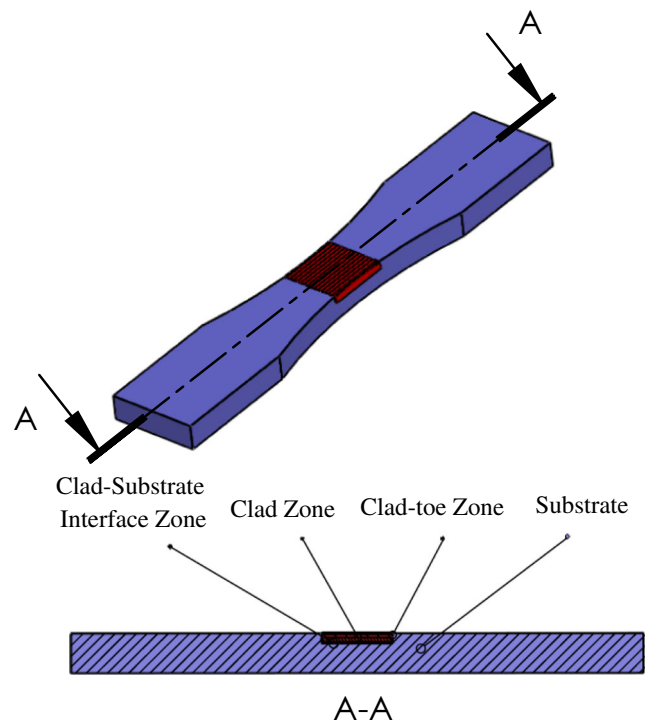
Parameter	Value
Laser power	400 W
Laser beam diameter	1.5 mm
Powder feed rate	0.38 gr/s (Eq. 25 rpm disc speed)
Nozzle linear speed	2 mm/s
Carrier gas flow rate	25 L/min
Protecting gas flow rate	20 L/min

## 2.4 HCF tests on the LC specimens

To perform the uniaxial HCF tests on the as-received and LC specimens, an automated servo-hydraulic test machine was utilized. The stress ratio,  $R$  = the minimum stress/the maximum stress, was set to 0.1. The loading variation was in sinusoidal form. The carried-out uniaxial tensile test on samples made of the material according to the standard practice ASTM-E8 [25] resulted in 1150 MPa and 886 MPa for the ultimate and yield tensile strengths, respectively. The value of the exerted maximum tensile stress in HCF tests for each specimen is either 800, 700, or 600 MPa, where all are greater than half the tensile strength and lower than 80% of the yield stress. This has been set to ensure that the fatigue tests were conducted for the material in the best-fit linear in elastic region of the S-N curve. In Fig. 5, a specimen under the HCF test is shown.

## 2.5 Microstructural analysis of LC specimen preparation

To analyze thoroughly the microstructure of the LC specimens, some mounted samples, which correspond to the section of the LC specimens, are prepared. In Fig. 6, four different

**Fig. 5** High-cycle fatigue test on a specimen**Fig. 6** The four zones of SEM imaging: (a) the substrate zone, (b) the clad zone, (c) the clad-substrate interface zone, and (d) the clad-toe zone

zones, which are analyzed, are shown. These four zones include the substrate zone, the clad zone, the clad-substrate interface zone, and the clad-toe zone.

The samples were prepared first by cutting the pieces of the material from the cladded-area section and mounting them using a hot compression thermosetting resin. Then, the samples were polished in the usual way and finished on 0.5- $\mu\text{m}$  diamond paste. In the next step, to reveal the microstructure, the samples were etched using two separate etchants, given in Table 3. The etchant no. 1 was used to dissolve gamma prime  $\gamma'$  and gamma double prime  $\gamma''$  phases, and the etchant no. 2 (marble) to dissolve grain boundaries.

Microstructural analysis images are taken by a VEGA TESCAN™ SEM, and chemical analysis are done by energy-dispersive X-ray spectroscopy (EDS) with electron probe microanalysis (EPMA).

**Table 3** The two etchants used to reveal the microstructure

Etchant name	Composition
Inconel 718-specific etchant	10 ml. $\text{HNO}_3$ + 10 ml. $\text{C}_2\text{H}_4$ + 15 ml. HCl
Marble	20 ml. $\text{H}_2\text{O}$ + 20 ml. HCl + 6.4 gr $\text{CuSO}_4$



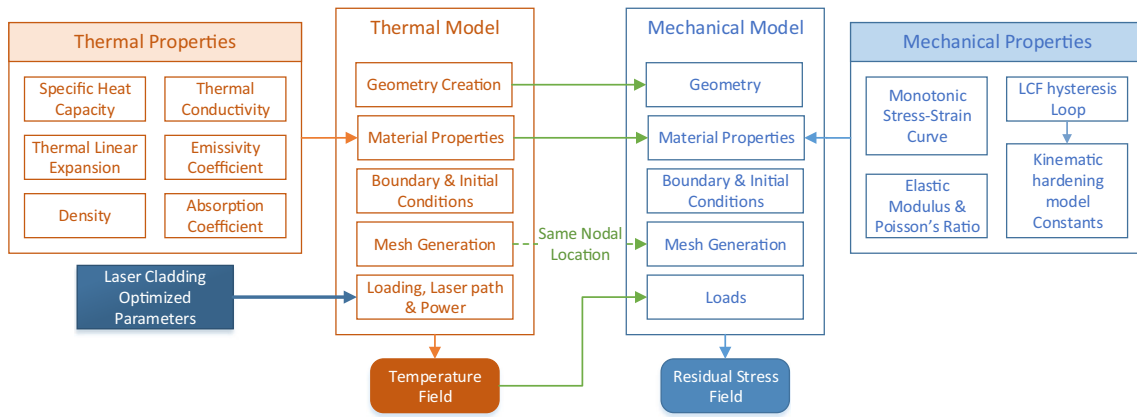


Fig. 7 The basic steps of the FE analysis to predict the residual stress distribution in the LC specimens

### 2.6 The finite element analysis

A finite element analysis (FEA) has been performed in order to obtain the residual stress distribution created in the specimens as a result of the laser-cladding process. The basic steps of the FE analysis are depicted in Fig. 7.

### 2.7 The material properties used in the FEA

Material properties needed for the thermomechanical analysis are generally temperature dependent. The values of the four material properties, including the specific heat capacity, thermal conductivity, thermal linear expansion, and emissivity coefficient, used in the first stage of the FEA, i.e., the thermal stage, for the material Inconel 718 are depicted versus temperature in Fig. 8.

The fusion latent heat for the material was assumed to be 241 J/kg [27]. The solidification and melting points of the material, which determine its melting range, were also assumed as 1260 and 1336 °C, respectively. Moreover, the value for the laser absorption coefficient of the material was considered as 0.35 [28], and the material density was assumed to be 8224 kg/m<sup>3</sup> [27].

For the mechanical analysis, some material properties, including the modulus of elasticity, Poisson’s ratio, yield strength, ultimate tensile strength, and fracture strain, are needed. The results listed in Table 4 were obtained from the uniaxial tensile test,

Table 4 Temperature-dependent mechanical properties obtained from the tensile test

Parameter	Temperature (°C)		
	Room temp.	649	760
Modulus of elasticity ( <i>E</i> ) [GPa]	199.9	163.4	153.8
Poisson’s ratio ( <i>ν</i> )	0.294	0.283	0.306
Yield strength ( <i>S<sub>y</sub></i> ) [MPa]	886	781	573
Ultimate tensile strength ( <i>S<sub>UTS</sub></i> ) [MPa]	1150	920	596
Fracture strain ( <i>ε<sub>f</sub></i> ) [m/m]	0.31	0.19	0.13

carried out according to the standard practice ASTM-E8 [25], on samples made out of the material Inconel 718 at three different temperatures.

Finite element results with the use of the material properties presented in Table 4 are called “conventional” in order to distinguish with cyclic plasticity finite element analysis. As an important fact, the plastic behavior of high-strength materials like Inconel 718 under a cyclic loading is significantly different from the behavior in the corresponding monotonic loading [29, 30]. Besides this, in the laser-cladding process, the cyclic thermal loading is present which produces cyclic stresses in the specimens. Hence, analyzing the mechanical behavior of Inconel 718 based on an appropriate cyclic plasticity model would be vital. Therefore, the non-linear kinematic hardening behavior [23] was here also utilized in the FE analysis.

In a kinematic hardening model, the yield surface is described by:

$$f = J(\sigma - \alpha) - K, \tag{1}$$

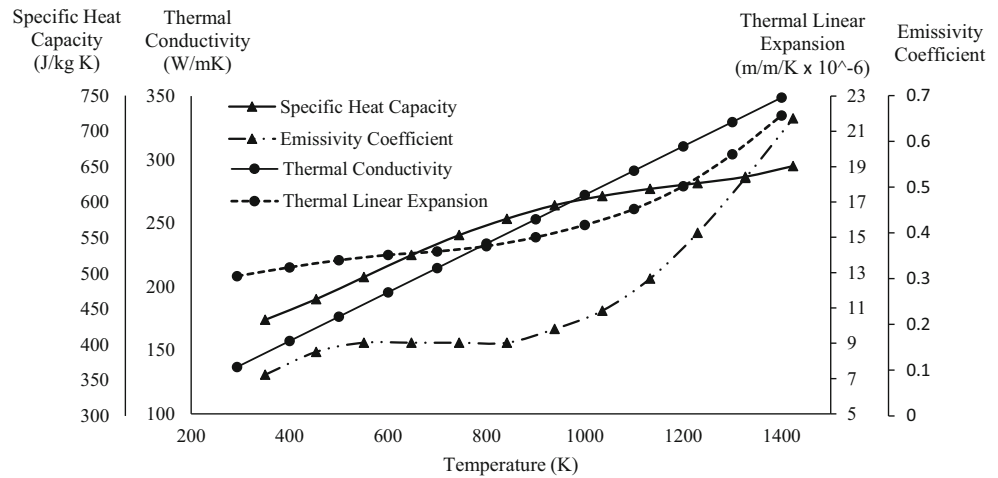
where  $\alpha$  is the back stress tensor that determines the center of the yield surface and  $K$  is a scalar that specifies the size of the yield surface. Moreover,  $\sigma$  denotes the Cauchy stress tensor, and scalar-valued function  $J$  gives the second principal invariant of the deviatoric part of its tensor argument. According to the Chaboche non-linear kinematic hardening model, the increment of the back stress tensor  $\alpha$  is written as:

$$d\alpha = \frac{2}{3} C d\varepsilon^P - \gamma \alpha dp, \tag{2}$$

where  $C$  and  $\gamma$  are material constants which are determined by experiments for a specific material. And,  $dp$  called the increment of the accumulated plastic strain is written as:

$$dp = \left( \frac{2}{3} d\varepsilon^P : d\varepsilon^P \right)^{\frac{1}{2}} \tag{3}$$

**Fig. 8** Temperature-dependent thermal properties [26, 27]



In order to determine the values of  $C$  and  $\gamma$  for Inconel 718 to be used in the FE analysis, low-cycle fatigue experiments according to ASTM E606 [31] were conducted. The low-cycle fatigue is needed to acquire a saturated hysteresis loop. The experiments were conducted for three different ranges of strain to get three saturated hysteresis loops. From these loops and by curve fitting,  $C$  and  $\gamma$  for Inconel 718 were determined to be 27,152 MPa and 3.43, respectively.

### 2.8 Residual stress measurement

In order to verify the obtained results of the FEA, the residual stress components  $S_{11}$  and  $S_{22}$  were measured at points with different depths on the substrate surface near the clad-toe zone of one of the specimens with the aid of the experimental method of incremental center hole drilling (ICHD). In the conducted ICHD, strains were measured by a Micro-Measurement strainmeter connected to a 1/16" standard TML rosette strain gauge. Based on the measured data for strains, the residual stresses were calculated based on the procedures presented in [32].

### 2.9 The shot peening procedure and fatigue tests on the shot-peened specimens

As indicated above, following laser cladding, the clad-toe zone becomes prone to fatigue damages because of significant tensile residual stresses and microstructural weakness in the zone. The

**Table 5** Shot peening parameters for the Almen intensity 18 A and 500% coverage

Parameter	Value
Media	S280
Air pressure [bar]	3.44
Time to reach 98% coverage [s]	26
Time to reach 500% coverage [s]	130

shot peening post-process eliminates the tensile residual stresses and transforms them to compressive nature. In addition, the severe shot peening enhances microstructures near the surface by grain refinement.

To investigate experimentally the effectiveness of the shot peening process, the fatigue life of LC specimens on different stress levels were carried out.

The shot peening parameters should generally be selected appropriately to provide benefits on fatigue life of parts. The parameters include the media type, the Almen intensity  $A$ , and the coverage. The Almen intensity determines the shot peening degree of intensity. For coverages above 100%, the process time should be a multiple of the time needed to reach 98% coverage. In our conducted severe shot peening process, the Almen intensity was 18 A and we had 500% coverage with the parameter setting according to Table 5.

Fatigue tests were carried out on nine shot-peened laser-cladded (SPLC) specimens, three tests at each stress level. The fatigue tests were conducted the same as those for the as-received and LC specimens in Section 2.3.

## 3 Results and discussion

### 3.1 HCF results

The fatigue life of specimens from the conducted HCF tests is listed in Table 6 for both the as-received and LC specimens. It should be noted that for each type of specimen at a certain maximum stress, three separate tests have been conducted.

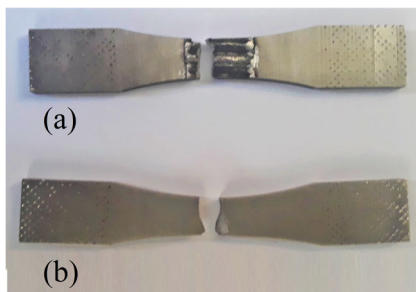
All LC specimens failed at clad-toe zone, i.e., at the top-surface boundary of cladding and substrate as it is depicted in Fig. 9, which shows the fractured as-received and LC specimens.

### 3.2 SEM and EDS results

The prepared samples were investigated by scanning electron microscopy. Also by conducting the energy-dispersive X-ray spectroscopy (EDS), the phase types at four different points on

**Table 6** The experimental results obtained for the fatigue life of LC and as-received specimens

Max. stress (MPa)		Fatigue life (cycles to failure, $\times 10^3$ )								
		600			700			800		
		Test 1	Test 2	Test 3	Test 1	Test 2	Test 3	Test 1	Test 2	Test 3
As-received specimens	Specimens	504	485	510	227	265	244	138	128	125
	Average		500			245			130	
	Standard error of the mean		7.5			11.0			3.9	
LC specimens	Specimens	445	410	401	170	163	175	76	68	81
	Average		419			169			75	
	Standard error of the mean		13.4			3.5			3.8	

**Fig. 9** Fractured specimens: **a** LC specimen and **b** as-received specimen

the substrate zone, the points shown in Fig. 10a, which depicts the SEM image of the zone, were determined. The phase types at points A, B, and C are simple and complex carbides, and at point D, the phase type is gamma double prime  $\gamma''$ . Table 7 shows the details of EDS analysis for these four points together with other points corresponding to the SEM figures depicted later in the paper. Figure 10b shows a separate area in the substrate zone. The phase type of point E on this figure was detected by EDS as Ti-rich carbide.

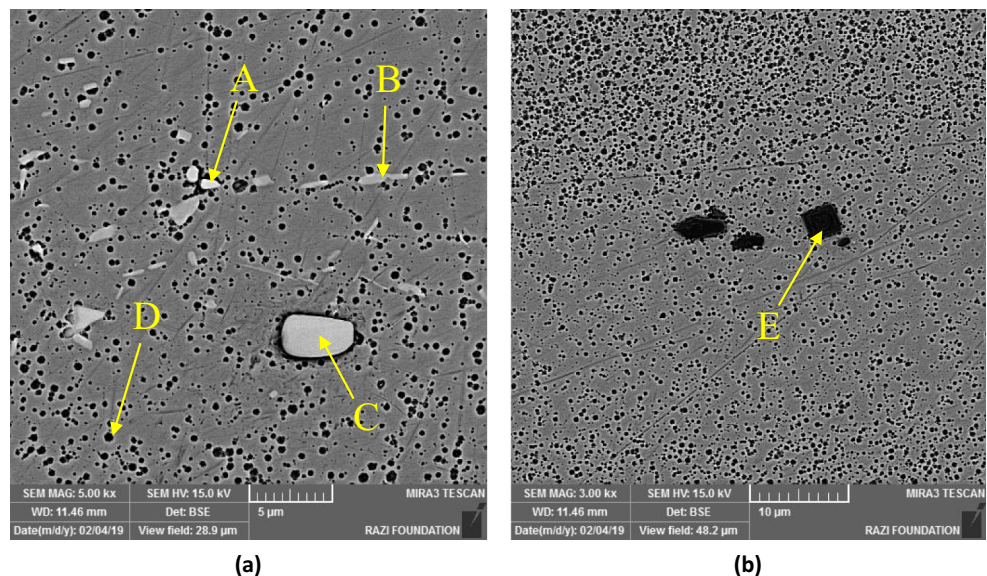
**Fig. 10** SEM images of the prepared samples of LC specimens demonstrating the microstructure at substrate. **a** MC carbides and gamma double prime  $\gamma''$  phase dispersed in the matrix and **b** Ti-rich carbides among gamma double prime phases

Figure 11a and b are SEM images of the clad zone. In the former, a dendritic structure can be seen in the zone, which is due to rapid cooling during the laser-cladding process. The phase types at points F, G, and H on these figures were determined to be mostly gamma double prime  $\gamma''$ , complex carbide, and simple carbide, respectively. The carbides in the clad zone are smaller in size comparing with those in the substrate zone, and they are here dispersed across the zone.

Figure 12 shows a SEM image from the clad-substrate interface zone. It indicates a metallurgical bond formation between the clad and substrate zones.

Figure 13a and b are SEM images of the clad-toe zone. As can be seen in the former, the presence of carbide phases is significantly higher in the interface of the clad and substrate zones comparing with those in the interface elsewhere. As another important fact can be seen in the latter, the diffusion of carbide phase from the clad zone into the substrate along a path is present. Given the brittle property of carbide phase, these two facts bring us to a conclusion that the clad-toe zone would be



**Table 7** Details of EDS analysis in different points in the substrate, clad zone, clad-substrate interface, and clad-toe zone shown in Figs. 10, 11, 12, and 13

Region	Point	Elements (wt%)								Composition	Phase designation
		Ni	Cr	Ti	Nb	Al	Mo	Fe	C		
Substrate	A	5.65	11.49	0.07	20.21	0.00	30.30	3.70	28.59	MC (Nb, Mo) and $M_7C_3$ , $M_6C$ , $M_{23}C_6$ (Cr)	Simple and complex carbides
	B	43.18	4.45	1.96	14.06	0.47	3.44	4.95	27.49	$M_7C_3$ , $M_6C$ , $M_{23}C_6$ (Ni) and MC (Nb)	Complex and simple carbides
	C	1.84	0.80	5.77	70.24	0.35	0.00	0.77	20.23	MC (Nb)	Simple carbide
	D	47.99	4.19	0.67	24.34	0.00	0.00	15.21	7.60	$Ni_3Nb$	Gamma double prime $\gamma''$
	E	0.90	0.73	70.07	04.38	0.41	0.00	0.16	23.34	MC (Ti-rich)	Ti-rich carbide
Clad zone	F	48.36	5.72	0.73	33.67	0.61	0.10	7.19	3.62	$Ni_3Nb$	Gamma double prime $\gamma''$
	G	21.08	10.38	4.31	10.12	2.84	4.33	7.96	38.97	$M_7C_3$ , $M_6C$ , $M_{23}C_6$ (Ni, Cr) and MC (Nb)	Complex and simple carbides
	H	30.33	10.82	1.13	17.38	0.54	0.44	10.40	28.95	MC (Nb) and $M_7C_3$ , $M_6C$ , $M_{23}C_6$ (Ni, Cr)	Complex and simple carbides
Clad-toe zone	I	2.04	0.79	65.35	5.37	0.39	3.26	0.70	22.10	MC (Ti-rich)	Ti-rich carbide
	J	1.89	0.78	7.86	64.48	0.40	3.78	0.84	19.98	MC (Nb)	Simple carbide
	K	31.13	0.86	35.47	8.27	18.43	1.07	0.50	4.26	$Ni_3(Al, Ti)$	Gamma prime $\gamma'$

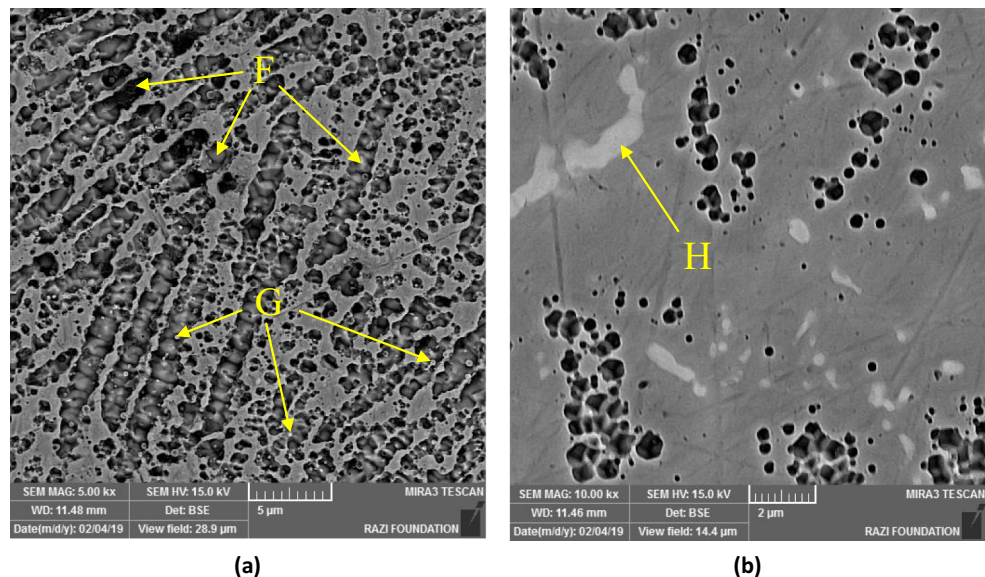
vulnerable to crack initiation, which makes it weak against the cyclic loadings with low fatigue performance. The phase types at points I, J, and K shown in Fig. 13a were determined to be Ti-rich carbide, simple carbide, and conglomerated gamma prime  $\gamma'$ , respectively. This presence of aggregated gamma prime  $\gamma'$  in the clad-toe zone, unlike the situation detected in other zones, provides another reason to expect that the clad-toe zone becomes prone to cyclic loading damage. It should also be recalled that HCF experiments described in the previous section have shown that the LC specimens all failed at the clad-toe zone.

### 3.3 Residual stress measurement results and comparison

In Figs. 14 and 15, the results for  $S_{11}$  and  $S_{22}$ , respectively, distribution along the thickness based on cyclic plasticity FEA, conventional plasticity FEA, and experimental ICHD are separately depicted.

It is clear that cyclic plasticity FEA results are in a good agreement with the experimental results. It would ensure that the carried-out FEA is valid and can be referred for the distribution of residual stresses with appropriate accuracy. It should

**Fig. 11** SEM images of the prepared samples of LC specimens demonstrating the microstructure at clad zone. **a** Dendritic structure of the clad zone, with gamma double prime  $\gamma''$  phases and dispersed small size carbides and **b** complex carbides in grain boundaries in the clad zone



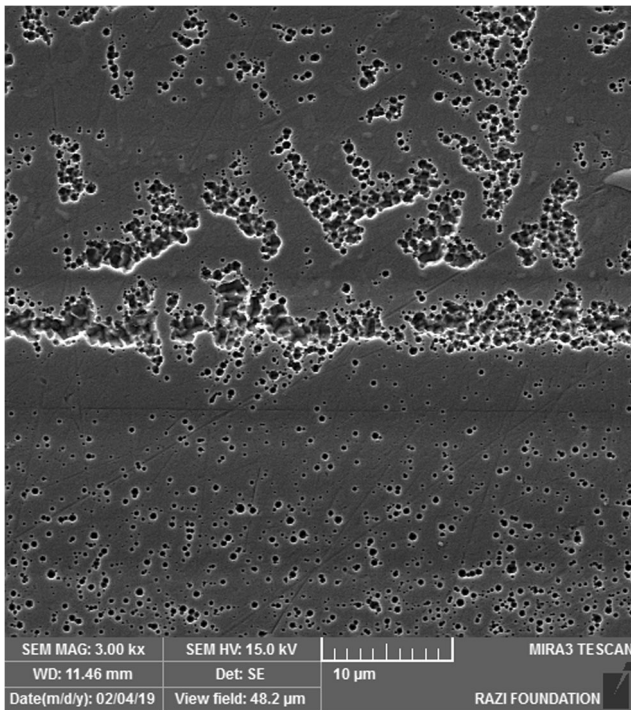


**Fig. 12** SEM images of the prepared samples of LC specimens demonstrating the microstructure at the clad-substrate interface showing a metallurgical bond formation

be noted that this accuracy for FEA is attainable only when the cyclic plasticity is utilized in the analysis, not the conventional plasticity.

### 3.4 FEA results

The FEA determines the distribution of components of the residual stress in the specimen. The distribution of the

**Fig. 13** SEM images of the prepared samples of LC specimens demonstrating the microstructure at clad-toe zone showing **a** the presence of carbides in this zone and gamma prime  $\gamma'$  aggregation, and **b** carbide diffusion from the clad zone into the substrate

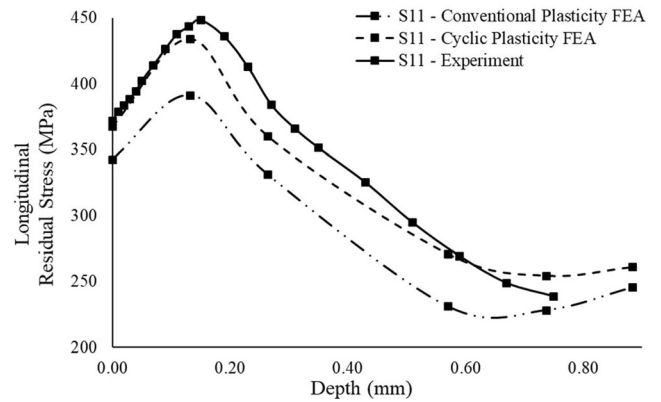
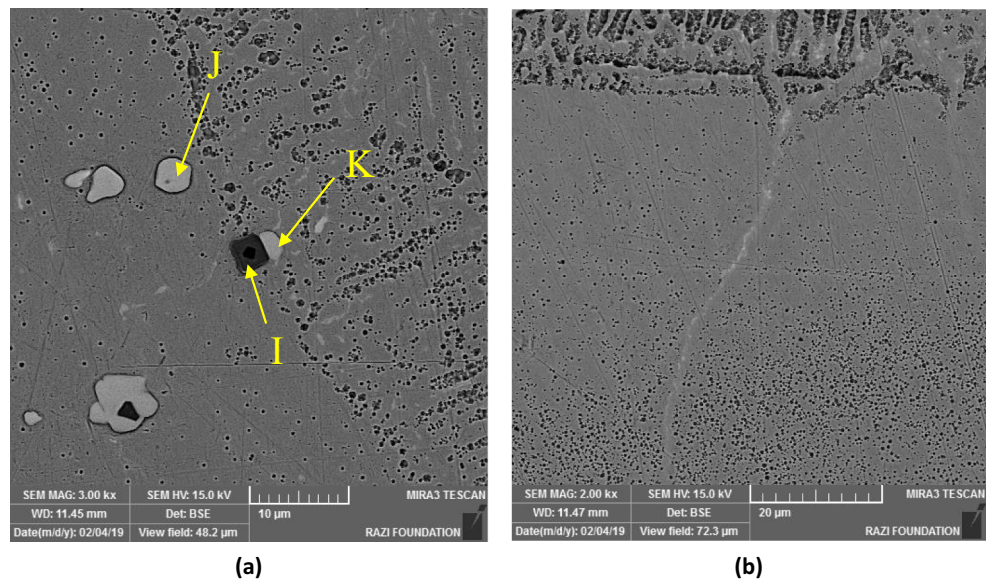


**Fig. 14** Longitudinal residual stress  $S_{11}$  distribution along the thickness at a point near the clad-toe zone

longitudinal component  $S_{11}$  and the transverse component  $S_{22}$  of the residual deviatoric stress tensor as well as the von-Mises equivalent stress in the LC specimen is depicted in Fig. 16 based on the cyclic hardening model. It is clear that at the clad-toe zone,  $S_{11}$  and  $S_{22}$  are tensile, and each is at their own maximum value. It should be noted that at this zone, the von-Mises equivalent stress is at its maximum value, too. These observations are in agreement with the HCF test results which indicated that all LC specimens failed at the clad-toe zone. It should be recalled that the carried-out microstructure analysis also provided indications that the clad-toe zone is vulnerable to fail under cyclic loading.

### 3.5 Shot-peened laser-cladded specimens' analysis results

In order to get sure that severe shot peening effected on the surface of the specimens, optical microscope image was taken



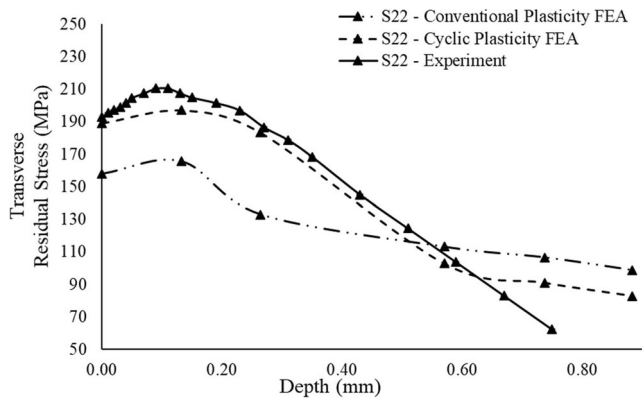


**Fig. 15** Transverse residual stress  $S_{22}$  distribution along the thickness at a point near the clad-toe zone

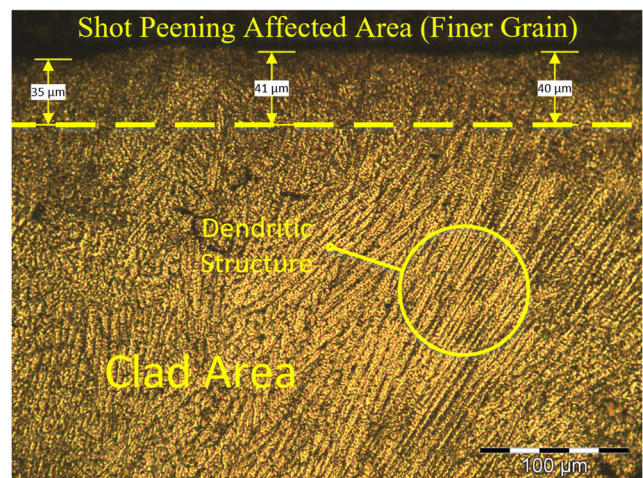


**Fig. 17** Grain refinement on the surface of the SPLC specimens

from the section of a SPLC specimen. The result is shown in Fig. 17.

In Fig. 18, the results of the conducted fatigue tests for the three categories of specimens, including the (a) as-received specimens, (b) LC specimens, and (c) SPLC specimens, are demonstrated. It is clear that the laser cladding has had a significant negative effect on the fatigue strength of

specimens, particularly at high values of the maximum stress, and that the shot peening post-processing has almost restored the fatigue strength for the specimens. This outcome emphasizes the great effectiveness of shot peening on the fatigue life of LC specimens. It should be noted that the fracture occurred at the clad-toe zone of all specimens in categories b and c.

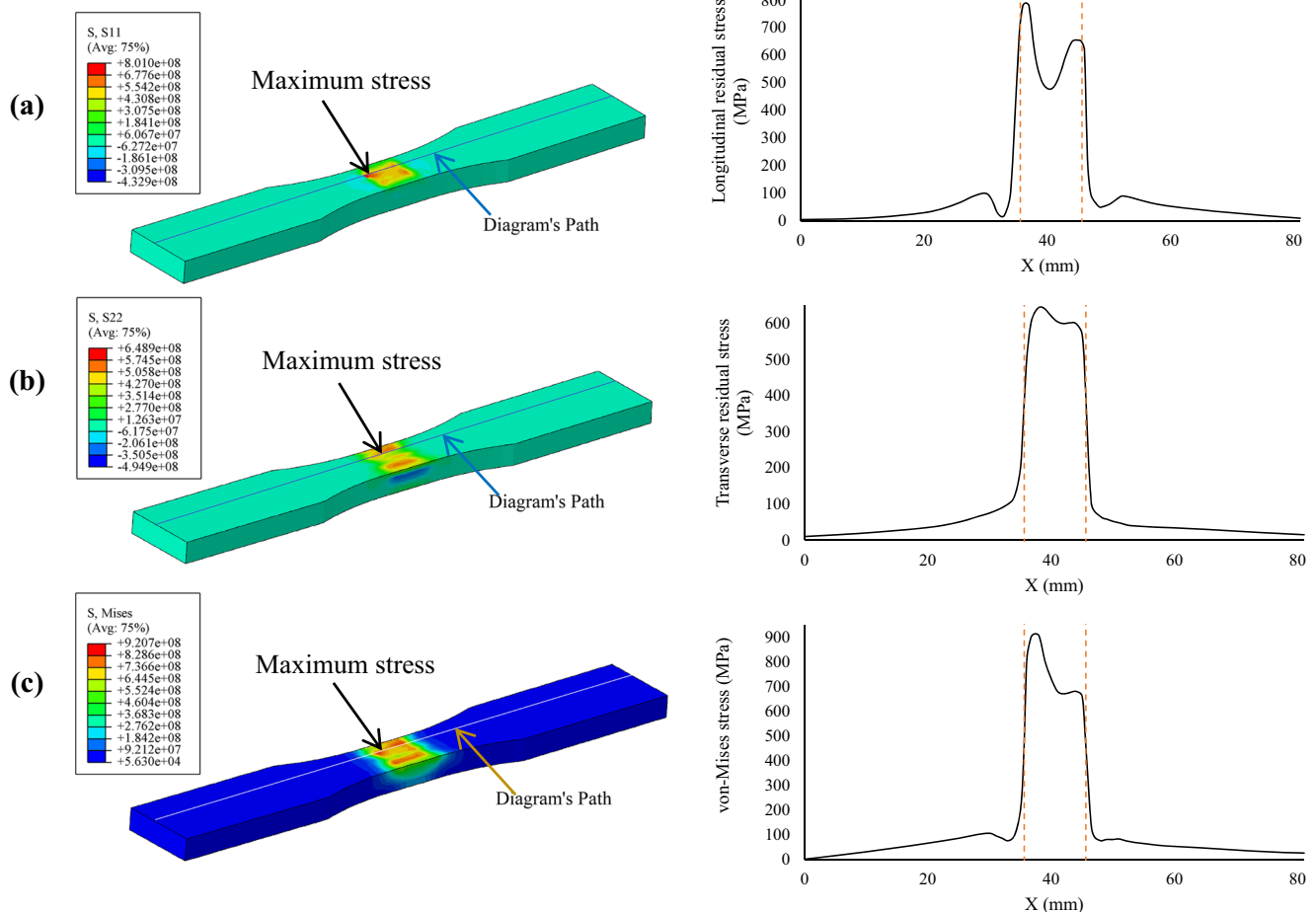


**Fig. 16** Residual stress component distributions in the LC specimens: **a**  $S_{11}$ , **b**  $S_{22}$ , and **c** the von-Mises stress

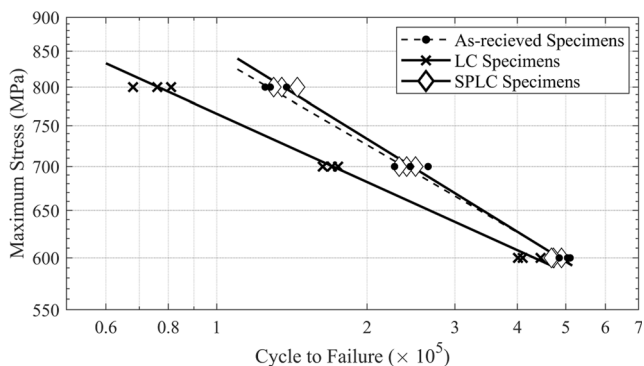


**Fig. 18** The maximum stress versus the cycles to failure for the as-received, LC, and SPLC specimens

Luo et al. [10] also showed the same result on the fatigue strength of TC17 titanium alloy. They showed that substrate specimen and LC specimen have fatigue strength of 401 MPa and 365 MPa, respectively. By performing laser shock peening on the LC specimens, fatigue strength increased by 12.5% with respect to substrate specimens and reached 451 MPa. They proved by this investigation that a peening process can enhance the fatigue life of a LC specimen.

The fracture surfaces of specimens are shown in Fig. 19a–c, where a corresponds to an as-received specimen, b to an LC specimen, and c to a SPLC specimen. Figure 19a illustrates that the crack has initiated from a corner of the section of the as-received specimen, while for the as-clad specimen, as well as for the SPLC specimen, the crack has initiated from a point on the clad area of the section, as seen in Fig. 19b and c. It should be also recalled that according to the FEA results in Section 3.4, the maximum residual tensile stresses appear in the clad-toe zone of LC

specimens. This fact makes the clad-toe zone more vulnerable to crack initiation.

## 4 Conclusion

In the present work, the effectiveness of severe shot peening treatment on restoring the fatigue performance of the laser-clad (LC) Inconel 718 specimens has been experimentally investigated by conducting a series of uniaxial fatigue tests. Prior to this investigation, the detrimental effect of laser-cladding process on the fatigue strength of specimens was verified experimentally. This detrimental effect was also predicted by performing a finite element analysis (FEA) based on a cyclic plasticity model with non-linear kinematic hardening in order to assess the distribution of residual stresses caused by the laser-cladding process. This assessment of FEA for the residual stresses was experimentally verified by conducting incremental center hole drilling. It is worth noting that the performed microstructure analysis has indicated that in the clad-toe zone, the microstructures suffer some weakness due to the presence of more carbides compared with other areas and also diffusion of carbides into substrate. Aggregation of carbides as a brittle phase in this zone could make it prone to crack initiation in the cyclic loadings.

The present investigation reveals a major advantage of shot peening treatment for LC specimens in restoring their deteriorated fatigue strength caused by laser cladding. Particularly, at higher values for the maximum stress in fatigue tests, this deterioration was observed at significant amounts of about 40% in the conducted experiments; and this significant deterioration was almost restored by the conducted shot peening

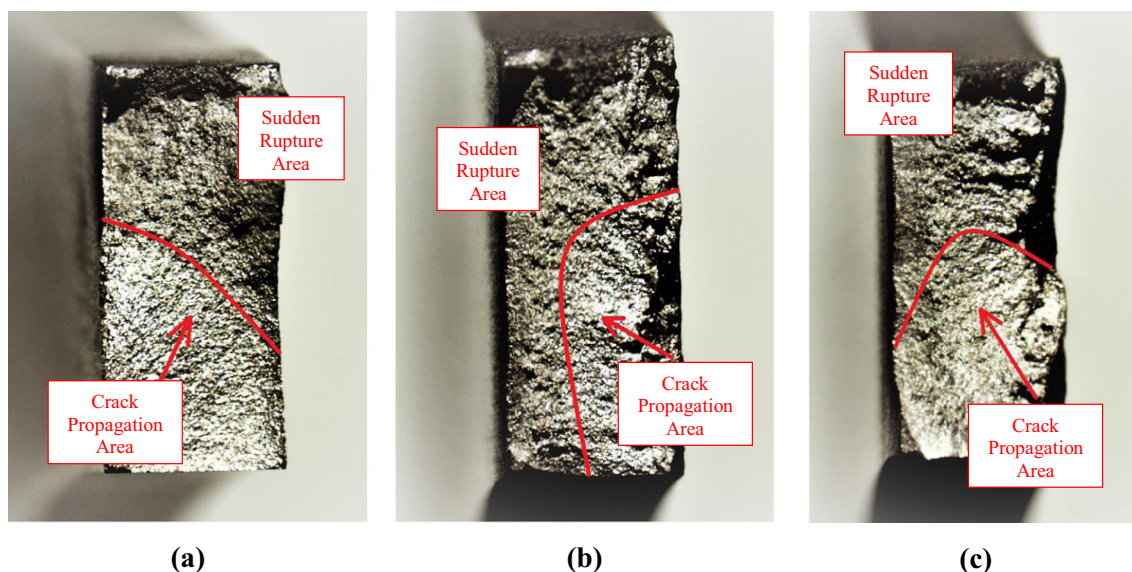


**Fig. 19** Fractography of the fracture surfaces of **a** an as-received specimen, **b** an LC specimen, and **c** a SPLC specimen



post-process. The usefulness of severe shot peening treatment in restoring the fatigue strength of LC specimens can be justified by the well-known facts of the occurrence of compressive residual stresses and the presence of grains with finer sizes near the surface after the treatment.

The results also indicate that the clad-toe zone is the weakest area concerning fatigue issues in all LC specimens with or without shot peening post-process. Thus, paying attention to this zone by pursuing activities like geometrical modification of the zone with chamfering or filleting would be promising.

## References

- Ganesh P, Kaul R, Paul CP et al (2010) Fatigue and fracture toughness characteristics of laser rapid manufactured Inconel 625 structures. *Mater Sci Eng A* 527:7490–7497
- Chew Y, Pang JHL (2016) Fatigue life prediction model for laser clad AISI 4340 specimens with multiple surface cracks. *Int J Fatigue* 87:235–244
- Tong X, Li F, Liu M et al (2010) Thermal fatigue resistance of non-smooth cast iron treated by laser cladding with different self-fluxing alloys. *Opt Laser Technol* 42:1154–1161
- Hutasoit N, Luzin V, Blicblau A et al (2015) Fatigue life of laser clad hardfacing alloys on AISI 4130 steel under rotary bending fatigue test. *Int J Fatigue* 72:42–52
- Lourenço JM, Da SS, Sharp K et al (2016) Fatigue and fracture behavior of laser clad repair of AerMet® 100 ultra-high strength steel. *Int J Fatigue* 85:18–30
- Chew Y, Pang JHL, Bi G, Song B (2017) Effects of laser cladding on fatigue performance of AISI 4340 steel in the as-clad and machine treated conditions. *J Mater Process Technol* 243:246–257
- Roy T, Lai Q, Abrahams R et al (2018) Effect of deposition material and heat treatment on wear and rolling contact fatigue of laser clad rails. *Wear* 412–413:69–81
- Klotz T, Delbergue D, Bocher P et al (2018) Surface characteristics and fatigue behavior of shot peened Inconel 718. *Int J Fatigue* 110:10–21
- Lainé SJ, Knowles KM, Doorbar PJ et al (2017) Microstructural characterisation of metallic shot peened and laser shock peened Ti–6Al–4V. *Acta Mater* 123:350–361
- Luo S, He W, Chen K et al (2018) Regain the fatigue strength of laser additive manufactured Ti alloy via laser shock peening. *J Alloys Compd* 750:626–635
- Zhuang W, Liu Q, Djugum R et al (2014) Deep surface rolling for fatigue life enhancement of laser clad aircraft aluminium alloy. *Appl Surf Sci* 320:558–562
- Ramos R, Ferreira N, Ferreira JAM et al (2016) Improvement in fatigue life of Al 7475-T7351 alloy specimens by applying ultrasonic and microshot peening. *Int J Fatigue* 92:87–95
- Zhang P, Lindemann J (2005) Influence of shot peening on high cycle fatigue properties of the high-strength wrought magnesium alloy AZ80. *Scr Mater* 52:485–490
- Bagherifard S, Guagliano M (2012) Fatigue behavior of a low-alloy steel with nanostructured surface obtained by severe shot peening. *Eng Fract Mech* 81:56–68
- Seddik R, Petit EJ, Rabii BS et al (2017) Predictive design approach of high-cycle fatigue limit of shot-peened parts. *Int J Adv Manuf Technol* 2321–2339(9):93
- Sidhom N, Laamouri A, Fathallah R et al (2005) Fatigue strength improvement of 5083 H11 Al-alloy T-welded joints by shot peening: experimental characterization and predictive approach. *Int J Fatigue* 27:729–745
- Habibi N, H-Gangaraj SM, Farrahi GH et al (2012) The effect of shot peening on fatigue life of welded tubular joint in offshore structure. *Mater Des* 36:250–257
- Lago J, Guagliano M, Bokůvka O et al (2017) Improvement of fatigue endurance of welded S355 J2 structural steel by severe shot peening. *Surf Eng* 33:715–720
- Benchouia S, Merakeb N, Adjel S et al (2019) Fatigue life enhancement of TIG-welded 304L stainless steels by shot peening. *Int J Adv Manuf Technol* 100:2885–2893
- Nazemi N, Urbanic J, Alam M (2017) Hardness and residual stress modeling of powder injection laser cladding of P420 coating on AISI 1018 substrate. *Int J Adv Manuf Technol* 93:3485–3503
- Shah K, Khurshid H, ul Haq I et al (2018) Numerical modelling of pulsed and continuous wave direct laser deposition of Ti-6Al-4V and Inconel 718. *Int J Adv Manuf Technol* 95:847–860
- Wang H, Yuan X, Wu K et al (2018) Effect of high energy shot-peening on the microstructure and mechanical properties of Al5052/Ti6Al4V lap joints. *J Mater Process Technol* 255:76–85
- Federick CO, Armstrong PJ (2007) A mathematical representation of the multiaxial Bauschinger effect. *Mater High Temp* 24:1–26
- (2007) ASTM E466-07, Standard Practice for Conducting Force Controlled Constant Amplitude Axial Fatigue Tests of Metallic Materials, ASTM International, West Conshohocken, PA, [www.astm.org](http://www.astm.org)
- (2004) ASTM E8-04, Standard Test Methods for Tension Testing of Metallic Materials, ASTM International, West Conshohocken, PA, [www.astm.org](http://www.astm.org)
- Davis JR (2000) ASM speciality handbook, Nickel cobalt and their alloys. ASM International, Materials Park
- Smith, G. D. and Baker, B. A. (2015). Nickel and Its Alloys. In *Mechanical Engineers' Handbook*, M. Kutz (Ed.), Wiley online library, <https://doi.org/10.1002/9781118985960.meh106>
- Gouge MF, Heigel JC, Michaleris P, Palmer TA (2015) Modeling forced convection in the thermal simulation of laser cladding processes. *Int J Adv Manuf Technol* 79:307–320
- PARK SJ, KIM KS, KIM HS (2007) Ratcheting behaviour and mean stress considerations in uniaxial low-cycle fatigue of Inconel 718 at 649 °C. *Fatigue Fract Eng Mater Struct* 30:1076–1083
- Xiao L, Chen DL, Chaturvedi MC (2008) Cyclic deformation mechanisms of precipitation-hardened Inconel 718 superalloy. *Mater Sci Eng A* 483–484:369–372
- (2004) ASTM / E606-04, Standard Practice for Strain-Controlled Fatigue Testing, ASTM International, West Conshohocken, PA, 2004, [www.astm.org](http://www.astm.org)
- Smith DJ, Farrahi GH, Zhu WX, McMahon CA (2001) Obtaining multiaxial residual stress distributions from limited measurements. *Mater Sci Eng A* 303:281–291

**Publisher's note** Springer Nature remains neutral with regard to jurisdictional claims in published maps and institutional affiliations.